This document is the accepted manuscript version of the following article:
Miller, S. R., Marshall, M. S. J., Wart, M., Crha, J., Trtik, P., & Nagarkar, V. V. (2020). High resolution thermal neutron imaging with 10Boron/CsI:Tl scintillator screen. IEEE Transactions on Nuclear Science, 1-1. https://doi.org/10.1109/TNS.2020.3006741

High Resolution Thermal Neutron Imaging with ^{10}Boron/CsI:Tl Scintillator Screen

Stuart R. Miller, Matthew S.J. Marshall, Megan Wart, Jan Crha, Pavel Trtik, and Vivek V. Nagarkar

***Abstract*–High resolution neutron imaging is difficult, due to the low-light output of neutron scintillators, and the spread of light within common neutron-sensitive scintillators as well as the spread of intermediate particles occurring during the detection process. To address this issue, we have developed a high-resolution scintillator for neutron imaging by combining enriched ^{10}B with the well-known CsI:Tl scintillator films. CsI:Tl has excellent properties for X-ray imaging applications, due to a high light yield of 60,000 photons/MeV, and high spatial resolution, which derives from its microcolumnar structure, which channels scintillation light to the photodetector. To enable CsI:Tl to detect neutrons, ^{10}B (96% enriched) was deposited by electron-beam directly onto the CsI:Tl film, making a layered scintillator structure in which the alphas produced by the neutron interaction with ^{10}B are detected in the CsI:Tl. The ^{10}B layer was approximately 3 µm thick, while the thickness of the CsI:Tl film was 11 µm. These novel layered scintillators were integrated into the high-resolution neutron imaging detector ('PSI Neutron Microscope') at the POLDI beamline at the Paul Scherer Institute (PSI). With our ^{10}B/CsI:Tl scintillator we were able to achieve a spatial resolution down to 9 µm. To demonstrate the effectiveness of the layered scintillator, we present results obtained by thermal neutron imaging as well as high-resolution neutron computed tomography. Finally, we believe there is considerable scope for future optimization of the performance of this system.**

***Index Terms*- microcolumnar scintillator, neutron radiography, neutron computed tomography, CsI:Tl, ^{10}B**

I. Introduction

High resolution neutron imaging is key objective for the neutron imaging community. While X-ray imaging routinely achieves submicron spatial resolution, neutron imaging has long been limited to resolution greater than 10 micrometers. In the past several years, detector advances have broken the 10 µm barrier and demonstrated spatial resolution down to 5 µm with the use of very thin ^{157}Gd-enriched gadolinium oxysulfide (Gd_2O_2S:Tb) films [1][2][3].

Here we have developed a high-resolution scintillator based on CsI:Tl which is well-known for its excellent material properties, and has found widespread use in many applications in both crystalline and thin film format. In particular, films grow in a needle-like structure that provide a combination of enhanced spatial resolution and high efficiency [4]. For cold or thermal neutron imaging, the columnar CsI:Tl can be combined with a neutron converter such as ^{10}B that absorbs neutrons to produce an alpha and a lithium ion. Previously we have shown that ^{6}LiF can be effectively combined with CsI:Tl for thermal neutron radiography [5].

^{10}B is of particular interest for high resolution neutron imaging for several reasons. First, ^{10}B has a high cross-section of 3,837 barns for thermal neutrons, which is more than four times higher than that of ^{6}Li (935 barns). Second, the products of the ^{10}B-neutron interaction are alphas and lithium ions with relatively low total energy of 2.31 MeV (94%)[6], which do not travel very far in the scintillator; this reduces image blur and enhances spatial resolution. Third, because ^{10}B material is black it serves as an optical absorber for stray light reflections, thereby enhancing spatial resolution [7]. While ^{155,157}Gd isotopes have higher neutron cross sections, the products of neutron capture include gamma photons and conversion electrons, which have the disadvantage of longer travel distances and therefore greater image blur.

The relatively low energies of the products of the neutron interaction in ^{10}B limit the optimal thickness of the ^{10}B coating to approximately 3 µm, or 0.7 mg/cm^2 [8]. While thicker layers would absorb more neutrons, these products do not escape the boron layer to reach the scintillator. The optimal thickness is calculated as the thickness that produces the highest number of alphas and lithium ions escaping the boron layer to reach the scintillator. Hence, the disadvantage of this approach is that the efficiency is limited to the 4-5% range [6][8].

In this study we have deposited 96% isotopically enriched ^{10}B onto the surface of thin CsI:Tl films as shown in Fig. 1. To enhance the resolution of the layered scintillator structure, the CsI:Tl layer was on the order of 11 µm thick, with columns beginning to form after approximately 4-5 µm of amorphous growth. On top of the ^{10}B layer is a coating of Parylene C (polyxylylene, from Uniglobe Kisko Inc.), which serves to protect against degradation by moisture. In order to enhance detection efficiency, we also introduced trenches in the CsI:Tl layer of one specimen by laser-cutting prior to ^{10}B deposition. The substrates for one sample was borosilicate glass, as shown in Fig. 1, while the second, laser-pixelated sample was on a fiberoptic faceplate.

Manuscript received December 10, 2019.

S. R. Miller, M. S. J. Marshall, M. Wart, and V. V. Nagarkar are with Radiation Monitoring Devices, Inc., Watertown, MA 02472 USA (e-mail: smiller@rmdinc.com.

J. Crha and P. Trtik are with the Laboratory for Neutron Scattering and Imaging, Paul Scherrer Institut, CH-5232 Villigen PSI, Switzerland and are both also associated with Czech Technical University in Prague, Prague, Czech Republic

978-1-5386-2282-7/17/$31.00 ©2017 IEEE

This article has been accepted for publication in a future issue of this journal, but has not been fully edited. Content may change prior to final publication. Citation information: DOI 10.1109/TNS.2020.3006741, IEEE Transactions on Nuclear Science

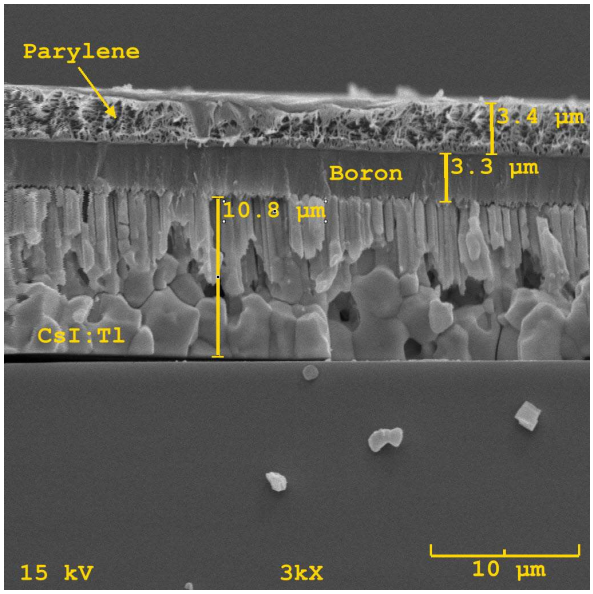

Fig. 1: SEM image showing 11 µm thick CsI:Tl film coated with a 3.3 µm thick enriched ^{10}B layer and then a 3.5 µm protective Parylene coating. Substrate is borosilicate glass.

II. Methods and Materials

A. Scintillator Screen Fabrication

For imaging measurements, microcolumnar CsI:Tl films were deposited by physical vapor film deposition methods onto glass or fiberoptic faceplates (FOP). The FOPs had a numerical aperture (NA) of 0.66 and 6 µm core diameters (type BFC89-6 from Incom) and contained statistical EMA (extra mural absorber). The 96% ^{10}B-enriched metal, obtained from Ceradyne Inc., was deposited onto the top surface of the CsI:Tl columnar films by e-beam deposition to a thickness of 3 µm, which was calculated to be in the optimal thickness range for balancing detection efficiency and maximizing signal to the photodetector. The structure of the screens used in this study, with the ^{10}B forming a distinct layer on top of the CsI:Tl columns, has been shown in Fig. 1.

Results from two samples are presented here, one with the ^{10}B layer deposited directly on the CsI:Tl as shown in Fig. 1, the second processed with a laser to produce pixels prior to coating with ^{10}B. The pixel pitch was 50 µm and groove widths on the order of 8 µm. A dark field image of the top surface was acquired with a with a Leica microscope at magnification of 200×, as shown in Fig. 2.

B. Evaluations

1) X-ray

Initial evaluations of the screens were performed with X-rays from a GE Senographe 600 mammography X-ray source using 28 kVp X-rays and a Mo anode with effective energy 17 keV. With these settings, the screens were coupled to a Photometrics camera consisting of a 1k × 1k CCD with a 3:1 fiberoptic taper. The effective pixel size is 57 µm and therefore a Nyquist limiting frequency of 8.8 lp/mm. The pre-sampling MTFs (Modulation Transfer Function) of the screens were measured by imaging a tantalum slit according to the technique described by Fujita *et al.*

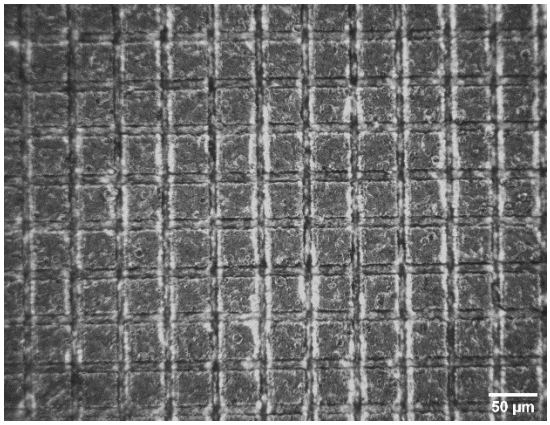

Fig. 2: Top view of the laser-cut CsI:Tl sample after boron coating showing laser cuts at 50 µm pitch with 8 µm wide grooves.

[9]. To measure the MTF(*f*), an image of a 10 µm wide slit made of 1.5 mm thick tantalum (placed at a slight angle (less than 4º) to the pixel matrix) was obtained.

Additional X-ray images were acquired by integrating the specimens in a high-resolution imaging system at RMD. The detector is an Andor EMCCD that is lens-coupled to the scintillator with high magnification optics to achieve an effective pixel size of 2.6 µm. Here the X-ray source was an Hamamatsu X-ray source (L8121-03 Microfocus) with 40 kVp X-rays.

2) Neutron Radiography

Imaging evaluations with thermal neutrons were carried out by integrating the selected scintillator samples into the 'PSI Neutron Microscope' (NM) imaging detector. The NM has been installed at the POLDI beamline at Paul Scherer Institute (PSI) and the incoming neutron beam has been collimated using pairs of slits to collimation ratio of 218 [10]. The NM employs high numerical aperture objective (NA=0.4) that provides 5-times magnification [11]. The scintillation light produced at the scintillator screen is captured via the objective using a 2048 x 2048 charged coupled device (iKon-L, Andor technology) with a pixel size of 13.5 micrometers. Consequently, the resulting FoV of the image corresponds to area of 5.5 mm x 5.5 mm and the size of the individual pixel equals 2.7 micrometers. Images of a Siemens star test object were acquired to determine spatial resolution capability of each specimen when imaged with neutrons [12]. The star was made by depositing Gd, which has a high neutron cross-section, onto a glass substrate. Image acquisition times were 60 seconds, and flat-field correction was applied to remove fixed-pattern noise.

3) Neutron Microtomography

Using the same imaging detector equipped with the described scintillator screen, neutron microtomography was demonstrated by imaging a gold cup containing two 500 µm gold spheres [13]. The specimen was placed on a rotational stage and imaged at 0.53° increments, producing a complete dataset of 674 projected radiographs. The images were acquired with 2×2 binning (pixel size 5.4 micrometers) with 60s acquisition time. The projections were reconstructed with a Filtered-Back Projection (FBP) technique using a commercial program called Octopus Reconstruction (by Octopus Imaging Software) to

produce reconstructed 3D volumetric data and image slices [14].

III. Results & Discussion

A. X-ray Imaging

As described above, the spatial resolution of the scintillator samples was evaluated with relatively low energy X-rays. Very high spatial resolution was observed in the screens as shown in Fig. 3. Here we see that there is an increase in spatial resolution with the ^{10}B coating, whose absorption of stray light results in the observed increase in MTF(*f*). Indeed we observe an MTF(*f*) value of 50% at 6.7 lp/mm and 30% at 11 lp/mm (which corresponds to 45 µm resolution) a value better than the theoretical capability of our system, whose Nyquist limiting frequency is only 8.8 lp/mm.

In the high-resolution X-ray imaging system, both specimens produced excellent high-quality, high-resolution images. The image of the line-pair phantom is shown in Fig. 4 along with a line profile at 20 lp/mm. Here a contrast transfer function (CTF)

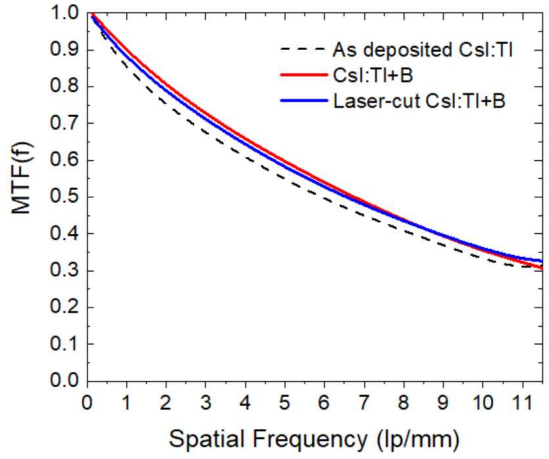

Fig. 3: Spatial resolution in terms of MTF(*f*) measured with X-rays for three CsI:Tl screens deposited on fiberoptic faceplates with EMA, including as-deposited, with ^{10}B coating, and laser-cut with ^{10}B coating.

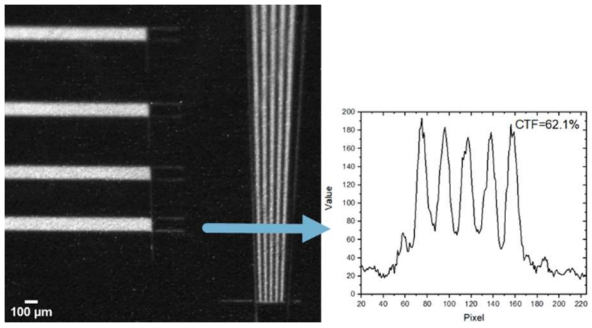

Fig. 4: X-ray image of a lead line-pair phantom acquired with the unpixelated ^{10}B/CsI:Tl specimen and RMD's high-resolution imaging system. Inset shows the line-pair profile at 20 lp/mm (25 µm) and CTF of 62%.

of 62% is observed at 20 lp/mm which corresponds to 25 µm spatial resolution. Clearly the limiting resolution is well beyond this value.

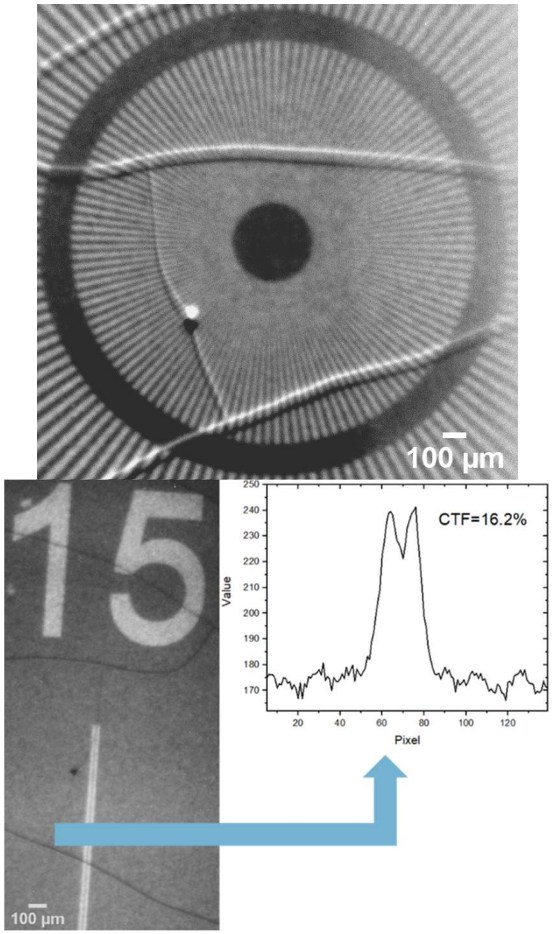

Fig. 5: (top) Cropped image of a Siemens star acquired with the ^{10}B/CsI:Tl scintillator screen integrated into the high-resolution imaging system at POLDI. (bottom) Image of a line-pair phantom with 15 micrometer resolution. Inset shows the line-pair profile and CTF of 16%.

B. Neutron Imaging

As described above, the scintillator specimens were integrated into the NM for neutron imaging evaluations. Both the laser-pixelated and the non-pixelated samples performed similarly, with very high spatial resolution observed. An image of the high-resolution Siemens star is shown in Fig. 5 (top). The spoke size in the inner circle goes from 24 micrometers to 4.5 micrometers closest to the center. The image has been flat-field corrected, however unfortunately the screen had moved slightly during this process, which accentuates physical cracks in the ^{10}B coating layer. Nonetheless, we observe a resolution of approximately 9 micrometers by the visual assessment of the narrowest observable spokes in the Siemens star. In Fig. 5 (bottom) a line-pair phantom image is shown with 15 µm spacing corresponding to 33 lp/mm. The CTF was calculated to be 16% at this frequency.

The Siemens star image acquired with the laser-cut sample is shown in Fig. 6 (top). The imaging performance is very similar to that of the unpixelated sample. The image has been acquired with a 10 minute acquisition time (10 acquisitions of 60 seconds) and therefore is noisier than the image the using non-pixelated scintillator. This is confirmed by the signal to noise (SNR) ratio calculated for the laser-cut screen which was 19.2

This article has been accepted for publication in a future issue of this journal, but has not been fully edited. Content may change prior to final publication. Citation information: DOI 10.1109/TNS.2020.3006741, IEEE Transactions on Nuclear Science

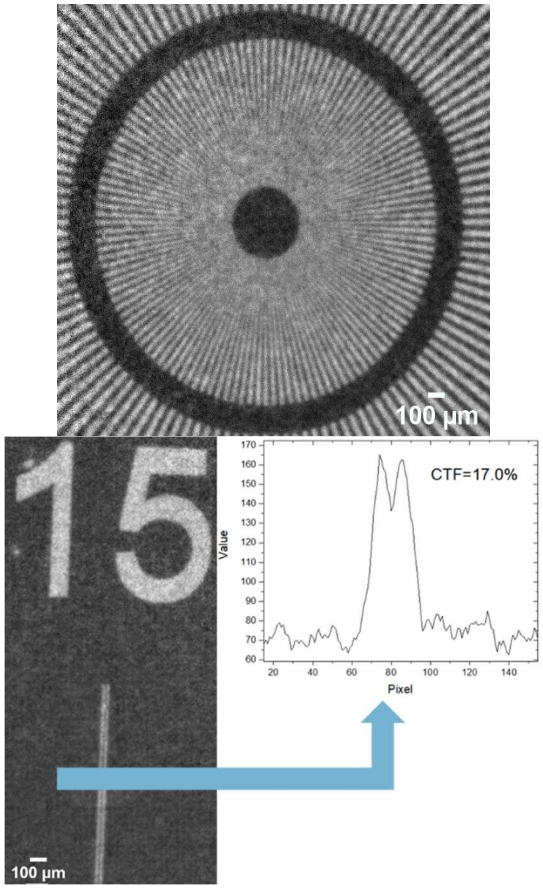

Fig. 6: (top) Same as Fig. 5 except acquired with the laser-cut screen into 50 µm pixels as illustrated in Fig. 2. The CTF here is slightly better, at 17 %.

versus 21.6 for the non-pixelated screen. The Fourier Ring Correlation (FRC) of the Siemens star image presented in Figure 6 was evaluated to be 11.7 µm, which corresponds rather well to the visually observable spoke size in the image (9 µm). Due to the above-mentioned motion artifact in the flat field image FRC couldn't be evaluated for the non-pixelated scintillator in Figure 5. The FRC resolution value for the image using pixelated scintillator can be well compared with the FRC value of 6.9 µm [15] of the same test object using similar test arrangement with scintillator screen based on ^{157}Gd-enriched gadolinium oxysulfide (Gd_2O_2S:Tb). The lower FRC resolution value of the ^{10}B screen reported here can be partly attributed to shorter acquisition times. The line-pair phantom image at the bottom of Fig. 6 has a measured CTF of 17%.

Light yield was also measured to be 221 ADU's (analog to digital units) for the non-pixelated screen and 189 for the pixelated. The former was deposited on a borosilicate glass substrate however, while the pixelated sample was on a FOP with EMA that substantially reduced light transmission.

C. Neutron Microtomography

Using the unpixelated screen from Fig. 5 the gold cup with spheres was imaged as described above. The cylindrical gold cup has a diameter of 1.5 mm with an opening at the top that is

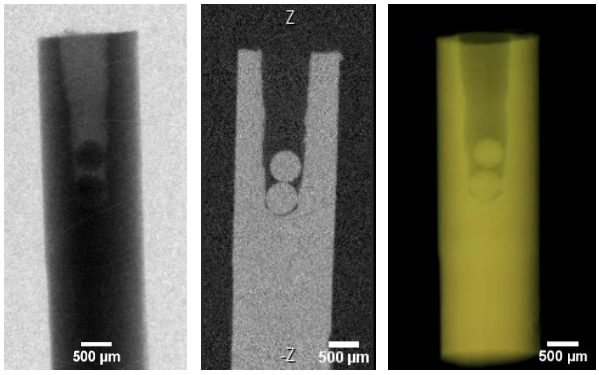

Fig. 7: Left, a single neutron radiograph of ~500 µm diameter gold spheres inside a gold cylinder; center, a single slice through the reconstructed volume; right, a 3-D view of the reconstructed volume.

approximately 0.75 mm in diameter. The depth of the hollow portion of the cup is 2.5 mm.

The resulting images of the gold cup are shown in Fig. 7. Shown here is a single radiograph as well as a reconstructed slice through the center of the object. The 3D volumetric view is also shown. The high quality, high-resolution images demonstrate capability of the Boron/CsI:Tl scintillator screen in imaging gold voids with excellent detail.

IV. Conclusion

To make a new, high resolution neutron scintillator we have combined the high neutron absorption of ^{10}B with the excellent scintillation properties of CsI:Tl by applying a thin layer of enriched ^{10}B on top of a microcolumnar CsI:Tl scintillator. The ^{10}B absorbs and converts the neutrons into secondary radiation (alphas & lithium ions), which is then converted into scintillation light by the CsI:Tl layer. Because the boron metal layer is also a black absorptive coating, this further enhances spatial resolution by reducing light spread, while also reducing the random light signal to the detector. This approach is effective in achieving high-resolution imaging although detection efficiency is limited to ~5% because with thicker layers (greater than 3.6 µm) of ^{10}B the secondary radiation can't reach the scintillator layer. To achieve higher detection efficiency we laser-pixelated one specimen, however, it is difficult to conclude whether higher light yield was observed since specimens were mounted on different substrate types.

The high-performance neutron scintillator screen was successfully demonstrated for neutron microtomography by imaging a small gold cup with spheres. There are several options for future developments and improvements in performance. For example, through enhancements in the deposition process to improve the structure of the of these very thin CsI:Tl films. Additionally the laser-treatment could be done with finer pitch and smaller grooves without cutting all the way through the CsI:Tl layer. This would provide greater surface area for the ^{10}B and hence improve detection efficiency.

Acknowledgment

This work is based on experiments performed at the Swiss spallation neutron source SINQ, Paul Scherrer Institute, Villigen, Switzerland.

REFERENCES

[1] P. Trtik, E.H. Lehmann, "Isotopically-enriched gadolinium-157 oxysulfide scintillator screens for the high-resolution neutron imaging," Nucl. Instrum. Methods Phys. Res. Sect. A Accel. Spectrom. Detect. Assoc. Equip., 788, 2015.

[2] J. Crha, et al, "Light Yield Enhancement of 157-Gadolinium Oxysulfide Scintillator Screens for the High-Resolution Neutron Imaging," MethodsX, vol. 6, pp. 107-114, 2019.

[3] P. Trtik, M. Meyer, T. Wehmann, A. Tengattini, D. Atkins, E. H. Lehmann and M. Strobl, PSI 'Neutron Microscope' at ILL-D50 beamline - first results," Materials Research Proceedings, Vol. 15, pp 23-28, 2020.

[4] S.R. Miller, V. Gaysinsky, I. Shestakova, V.V. Nagarkar, "Recent advances in columnar CsI:Tl scintillator screens," Proc. of SPIE, 5923, pp. 0F-1 - 0F-10, 2005.

[5] S.R. Miller, et al., "LiF/CsI:Tl Scintillator for High-Resolution Neutron Imaging," IEEE TNS Vol. 66, Issue 10, pp 2261-2264, 2019.

[6] Knoll G. F., Radiation Detection and Measurement, Fourth Edition, John Wiley & Sons, Inc., 2010, ISBN 978-0-470-13148-0.

[7] Nagarkar, V., Gupta, T.K., Miller, S., Klugerman, Y, Squillante, M.R. Structured CsI(Tl) Scintillators for X-ray Imaging Applications, IEEE Trans. Nucl. Sci., Vol. 45, No.3, pp. 492-496, June 1998.

[8] J. Uher, "3D neutron detectors," Doctoral Thesis, Institute of Experimental and Applied Physics, Czech Technical University, 2007.

[9] Fujita H., Tsai D.Y, Itoh T., Doi K., Morishita J., Ueda K., and Ohtsuka A., "A simple method for determining the modulation transfer function in digital radiography," IEEE Trans. Med. Imaging, 11, pp 34-39, 1992.

[10] U. Stuhr, et al., "Time-of-flight diffraction with multiple frame overlap Part II: the strain scanner POLDI at PSI," Nucl. Instrum. Methods Phys. Res. Sect. A Accel. Spectrom. Detect. Assoc. Equip., 545, pp. 330-338, 2005.

[11] P. Trtik, E.H. Lehmann, "Progress in High-resolution Neutron Imaging at the Paul Scherrer Institut - The Neutron Microscope Project," J. Phys. Conf. Ser., 746 (Sep. (1)) , pp. 012004, 2016.

[12] C. Grünzweig, G. Frei, E. Lehmann, G. Kühne, C. David, "Highly absorbing gadolinium test device to characterize the performance of neutron imaging detector systems," Rev. Sci. Instrum., 78 (5), 2007.

[13] Trtik, P. "Neutron microtomography of voids in gold," MethodsX, vol. 4, pp. 492-497, 2017.

[14] Vlassenbroeck, M. Dierick, B. Masschaele, V. Cnudde, L. Van Hoorebke, and P. Jacobs, "Software Tools for Quantification of X-ray Microtomography," Nucl. Instrum. Methods Phys. Res. A 580, pp 442-445, 2007.

[15] Gong, W, P.Trtik, A.W.Colldeweih, L.I.Duarte, M.Grosse, E.Lehmann, J.Bertsch, "Hydrogen diffusion and precipitation in duplex zirconium nuclear fuel cladding quantified by high-resolution neutron imaging," J. Nuclear Materials, vol, 526, 151757, 2019.